BeBeC-2018-D11

Phase coherence imaging of vibroacoustic sources

Maxime Bilodeau, Nicolas Quaegebeur, Alain Berry and Patrice Masson
Groupe d'Acoustique de l'Université de Sherbrooke, Dept. of Mechanical Engineering
Faculté de Génie, J1K 2R1, Sherbrooke, Canada
Email: maxime.bilodeau2@usherbrooke.ca

Abstract

The problem of identifying and localizing noise sources using microphone arrays led to a vast literature and numerous imaging algorithms in the field of vibroacoustics. However, the radiated acoustic power estimation of extended vibroacoustic sources is still challenging, due to the complex directivity and radiation patterns associated with such structures. The iterative algorithms and inverse formulations used in the last decade to estimate the radiated power from extended structures, typically result in large computational burden. The imaging algorithm presented herein aims at identifying the relative phase between individual monopoles on the whole imaging domain to help achieve better resolution in the identification of the boundaries of extended vibroacoustic sources. This highly parallelizable algorithm improves standard beamforming algorithms by using phase coherence filters and allows the identification of operational deflection shape of extended structures and better estimation of radiated acoustic power.

1 INTRODUCTION

1.1 Acoustic Imaging of extended sources

The problem of identifying multiple acoustic sources using imaging algorithms has been addressed by many authors in the past decades. However, identifying the boundaries of extended vibroacoustic sources in near field, their associated velocity field, and thus, the radiated acoustic power still challenges researchers [1]. Other approaches can be used to measure the radiated acoustic power of vibrating structures. Indeed, Near-Field Acoustic Holography (NAH) is an established method to characterize vibroacoustic sources, but the need to position a highly discretized microphone array very close to the structure of interest can be limitative [2]. Other non-contact approaches such as Laser Doppler Vibrometry and the use of p-u probes offer good precision, but are not suited for real time identification of transient phenomena or require precise calibration in controlled environments [3].

Consequently, acoustic imaging algorithms oriented toward the characterization of extended acoustic sources in the near-field have been presented in the litterature. However, the proposed algorithms are generally characterized by high complexity. Indeed they result in multidimensional optimization problems via the introduction of generalized steering vector or the use of multiple Green's functions [4, 5]. In order to avoid the need to introduce new source parameters such as shape or extend, a developed concept in ultrasound imaging, namely Phase Coherence (PC) could be adapted to the imaging of acoustic sources [6]. The origin of PC, its recent adaptation to the ultrasound domain and its potential in the audible domain are presented in Subsection 1.2.

1.2 Phase coherence

To help identifying low contrast sharp features in optics and image processing, various PC statistics can be used [7, 8]. Indeed, the importance of signal phase in the Fourier domain is a well known concept in optics and image processing [9]. Recently, the fact that phase carries the majority of a signal information was introduced in active ultrasound imaging through the use of PC filters for time-domain signals. It was shown that using PC filters in active ultrasound imaging, the number of insonifications and transducers can be reduced, resulting in shorter image computation time. The most efficient PC filters are metrics that quantify the similitude of the measured phase amongst the different receivers (transducers in ultrasound imaging). In other words, the images obtained using Beamforming (BF) principles are ponderated by spatial filters whose values are normalized by 1, depending on the strength of the phase coherence at each pixel. For instance, the Sign Coherence Factor (SCF) and the Circular Coherence Factor (CCF) are the most efficient PC filters to date [10]. Since PC statistics are known to increase sensitivity to edge detection (image processing) and to acoustic impedance variations (ultrasound imaging), one would be tempted to see if PC can help identifying the boundaries of noise sources in the audible domain.

Hence, based on the above PC filters, this article proposes an iterative PC algorithm for the passive imaging of stationary vibroacoustic sources in the frequency domain. As presented in the following, the use of PC amongst the different microphones of an array can help identifying the boundaries of extended acoustic sources. Following this identification process, an accurate estimation of the radiated acoustic power can be obtained.

2 Methodology

2.1 Array measurement and definitions

In the frequency domain, acoustic source identification can be performed using a set of acoustic pressure measurements. Given an active noise source, the acoustic pressure radiated at a given point in space can be expressed as a linear relationship from the normal velocity of this source. The analytical formulation of this principle is known as the Rayleigh integral. By discretizing the source domain in N source elements and assuming a constant velocity v_s over each element of a baffled planar vibrating structure, as presented in Figure 1, the Rayleigh integral can be expressed as the superposition of these N elements (given that the elements are smaller than the

acoustic and structural wavelengths):

$$p_m = p(x_m, y_m) = \frac{j\omega\rho_0}{2\pi} \sum_{s=1}^{N} v_s \frac{e^{-jkR_{ms}}}{R_{ms}} A_e \tag{1}$$

where p_m is the pressure measured by a microphone positioned at the cartesian coordinate (x_m, y_m, z_m), v_s is the normal complex velocity of the source element s of area A_e centered at (x_s, y_s, z_s), R_{ms} is the distance given by $\sqrt{(x_m - x_s)^2 + (y_m - y_s) + (z_m - z_s)^2}$, k is the wavenumber, ω is the angular frequency and ρ_0 the density of the medium [11]:

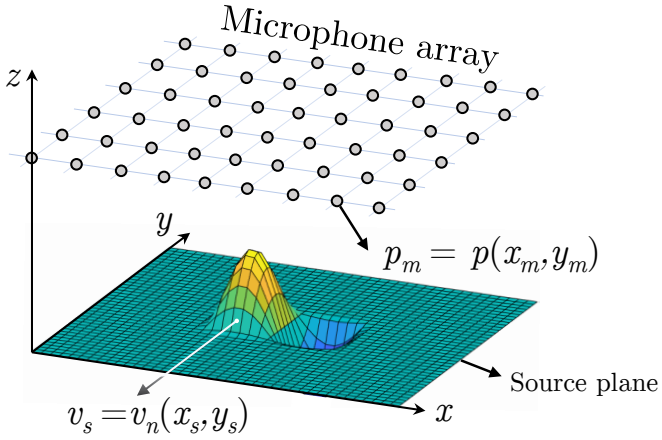

Figure 1: Acoustic pressure measured by an array of microphones positioned above an extended source represented by N source elements (monopoles)

Defining $G_{ms} = \frac{e^{-jkR_{ms}}}{R_{ms}}$ and separating the magnitude and phase of the complex velocity $v_s = |v_s| e^{j\phi_s}$, Eqn. 1 can be rewritten as the following system of linear equations:

$$\mathbf{P} = \frac{j\omega\rho_0 A_e}{2\pi} \underbrace{\begin{bmatrix} G_{11} & G_{12} & \dots & G_{1N} \\ G_{21} & G_{22} & & \vdots \\ \vdots & & \ddots & \\ G_{M1} & \dots & & G_{MN} \end{bmatrix}}_{[\mathbf{G}]} \begin{bmatrix} e^{j\phi_1} & 0 & \dots & 0 \\ 0 & e^{j\phi_2} & & \vdots \\ \vdots & & \ddots & \\ 0 & \dots & & e^{j\phi_N} \end{bmatrix} \underbrace{\begin{bmatrix} |v_1| \\ |v_2| \\ \vdots \\ |v_N| \end{bmatrix}}_{|\mathbf{v}|} \tag{2}$$

$$= \frac{j\omega\rho_0 A_e}{2\pi} [\mathbf{G}] \, \mathrm{diag}(e^{j\phi_1}, e^{j\phi_2}, \dots, e^{j\phi_N}) |\mathbf{v}| \tag{3}$$

where $[\mathbf{G}]$ is the $M \times N$ Green's matrix (M being the number of microphones), $\mathrm{diag}(e^{j\phi_1}, e^{j\phi_2}, \dots, e^{j\phi_N})$ is the $N \times N$ diagonal matrix containing the phase information of the source elements and $|\mathbf{v}|$ is the $N \times 1$ magnitude vector of the source elements normal velocity. The imaging algorithm proposed in the following section aims at first identifying the phase of every source element (or monopole) using beamforming principles, and then, reducing the imaging domain using a PC filter.

2.2 Iterative Phase Coherence Algorithm (iPCA)

Since most of the information of measured sound pressures is contained in the phase, a first identification of source velocity phase assuming an arbitrary source velocity magnitude should lead to a good first source identification [8]. Hence, using Beamforming (BF) priciples, the phase $\phi_{m,s}$ of each source element s can be evaluated by each microphone m under the assumption that only source element s contributes to the sound pressure at microphone m:

$$\phi_{m,s} = \arg\left(-jG^*_{ms}p_m\right) \tag{4}$$

where the real multiplicative factors from Eqn. 3 are neglected since only the argument is needed. For instance, the phasor ($e^{j\phi_{m,s}}$) evaluated by each microphone (m) for a given source pixel (s) is represented by a blue dot in Figure 2. The red arrow represents the phasor averaged over the microphone array in the case where the source pixel corresponds to an active source (Figure 2(a)) and when the source pixel corresponds to point of null velocity (Figure 2(b)).

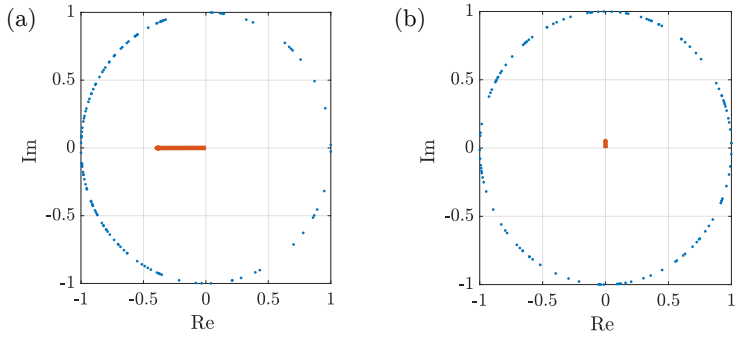

Figure 2: Phasor (blue dot) evaluated by each microphone for a given source pixel and the average (red arrow) of the M phasors. (a) Phasor identification of a source pixel that coincides with an active source ($\phi = \pi$) and (b) of a source pixel that does not coincide with any source.

Hence, the absolute phase of a given source pixel can be obtained by taking the argument of the phasor represented by the red arrow in Figure 2. It is clear that when an active source element coincides with the source pixel, the magnitude of the resulting mean phasor is greater than when no source is present. To help visualizing the phase coherence, the phases from Figure 2 can be represented in the form of an histogram, as presented in Figure 3.

In Figure 3, the maximum of the histogram for the wider strips shows that a strong phase coherence is obtained for the source pixel that coincides with the active source ($\phi \approx \pi$), whereas no clear phase coherence is measured for the other source pixel. Using this representation, the instantaneous phase of each source pixel can be estimated using the maximum of its associated histogram. Consequently, the magnitude of the average phasor presented in Figure 2 or the maximum of the histograms from Figure 3 can both be used to represent Phase Coherence (PC) between the different microphones for a given source pixel.

The PC is a useful tool to quantify the probability of source presence for a given pixel. Consequently, a threshold on the PC can be introduced to reject the source pixels associated

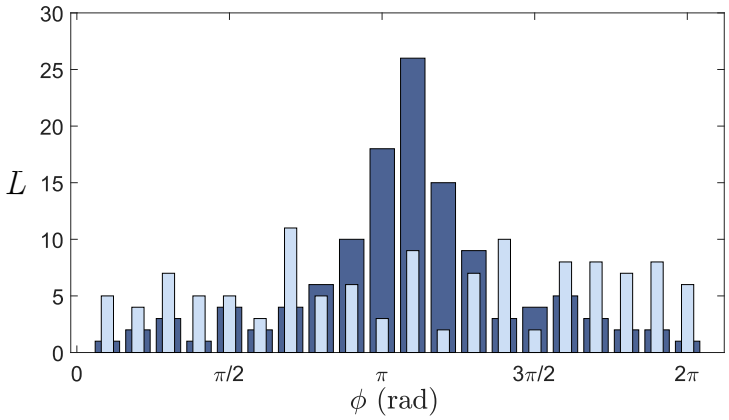

Figure 3: Source phase histogram as a function of number of microphones L in the array for a source pixel coinciding with an active source (wide strips) and with a zero source velocity (narrow strips)

to low source presence probability, resulting in a reduced imaging domain. Given the absolute phases (Eqn. 4) on this reduced imaging domain, the normal velocities can be calculated by substituting the obtained phases in Eqn. 3. Extracting the velocity field from Eqn. 3 using the Moore-Penrose pseudo inverse $(\cdot^{\dagger})$ of the Green's matrix $[\mathbf{G}]$, the following expression is obtained:

$$|\mathbf{v}| = \frac{2\pi}{j\omega\rho_0 A_e}\text{diag}(e^{-j\phi_1},...,e^{-j\phi_N})[\mathbf{G}]^{\dagger}\mathbf{P} \tag{5}$$

However, it is known that the poor conditionning of $[\mathbf{G}]$ is translated in an extreme sensitivity to noise. One solution to improve the conditionning of $[\mathbf{G}]$ is to solve Eqn. 5 using the Singular Value Decomposition (SVD) of $[\mathbf{G}]$. Using the SVD, the singular values associated to noise can be separated from the signal singular values, and even suppressed [12, 13]. This noise singular value rejection process is crucial to obtain a better conditionned $[\mathbf{G}]$ matrix, and thus, to obtain a correct evaluation of $\mathbf{v}$. However, the source velocity obtained using this technique can be further improved. Indeed, using an iterative process, the strength and usefulness of PC filtering is better put forward.

Instead of making the strong assumption of a unique active monopole source during the phase identification (as done in Eqn. 4), the whole domain (source plane) is considered using the superposition principle. Indeed, from an initial estimation of the velocity phase and magnitude for each source element, subsequent estimations of these quantities can be iteratively calculated with the consideration of superposition of all the source elements. Consequently, the phase of a given source pixel at iteration i can be evaluated from Eqn. 3 using the velocity phase and magnitude at all other source pixels from the previous iteration $(i-1)$:

$$\phi^i_{m,s} = \arg\left(\frac{p_m}{jf\rho_0 A_e} - \sum_{s'\neq s} G_{ms'}\cdot\exp\left(j\phi^{i-1}_{s'}\right)|v^{i-1}_s|\right) \tag{6}$$

where the velocity magnitude $|v^{i-1}_s|$ is calculated as in Eqn. 5 over the conserved pixels. At each iteration, the PC is recalculated and the imaging domain is modified based on the PC threshold.

To illustrate the rejection process, the number of pixels kept at different iterations is represented at Figure 4 for a given source configuration using a threshold of 10% on the phase coherence. The iteration process is repeated until convergence is obtained. The convergence criterion is defined by the convergence of the radiated power calculated by the method presented in the following section (section 2.3).

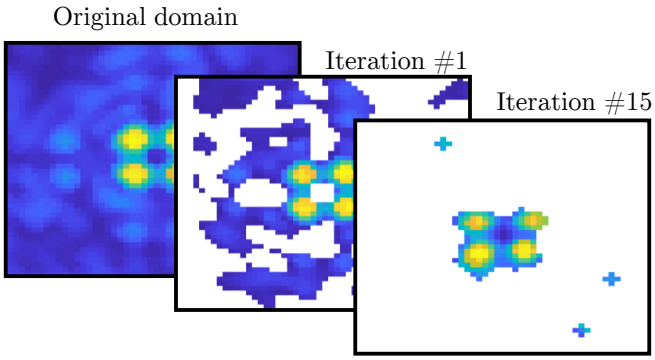

Figure 4: Evolution of the imaging domain at different iterations for the reconstruction of the complex normal velocity field (the white regions represent rejected pixels).

2.3 Radiated sound power

For a given vibrating structure of area S, the radiated acoustic power at a given angular frequency ω can be calculated by summing the contribution of each surface element of area (A_s) and is given by:

$$P = \frac{S}{2N}\Re\{\mathbf{v}^H\mathbf{p}\} \tag{7}$$

where $\mathbf{v}$ contains the normal velocity of each source element (column vector), $\mathbf{p}$ is the surface pressure acting on each source element (column vector) and the operator $(\cdot)^H$ is the conjugate transpose. As derived in [14], Eqn. 7 can be calculated using the radiation resistance matrix $[\mathbf{R}]$ and is given by:

$$P(\omega) = \mathbf{v}^H[\mathbf{R}]\mathbf{v} \tag{8}$$

with $[\mathbf{R}]$ defined as:

$$\mathbf{R} = \frac{\omega^2\rho_0 A_e^2}{4\pi c}\begin{bmatrix} 1 & \frac{\sin(kR_{12})}{kR_{12}} & \cdots & \frac{\sin(kR_{1N})}{kR_{1N}} \\ \frac{\sin(kR_{21})}{kR_{21}} & 1 & & \vdots \\ \vdots & & \ddots & \\ \frac{\sin(kR_{N1})}{kR_{N1}} & \cdots & & 1 \end{bmatrix} \tag{9}$$

where R_{ij} is the Euclidean distance between the source elements i and j The following section presents the numerical configurations considered to test the algorithm.

3 Results and discussion

3.1 Pistons

The first numerical configuration considered to test the algorithm is presented in Figure 5. Two square pistons of 0.3 m $\times$ 0.3 m, of identical amplitude (0.01 m), with a phase difference of $\pi/3$ are mounted on an infinite baffle and are included in the imaging domain (plane) considered.

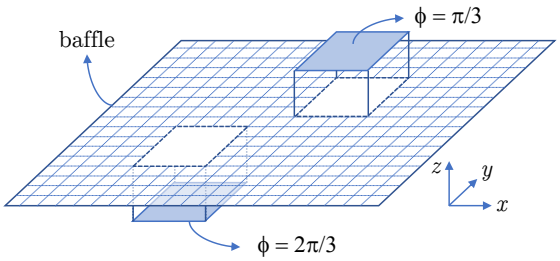

Figure 5: Stationnary sources for the numerical results : two pistons on an infinite baffle with a relative phase of $\pi/3$ (absolute phases : $\pi/3$ and $2\pi/3$)

A regular array of 121 microphones (11 $\times$ 11) is positioned at a distance of 0.8 m above the source plane as illustrated in Figure 1. The microphones, separated by 0.15 m, form an array of 1.5 m $\times$ 1.5 m. The imaging domain has the same dimensions and is discretized in a grid of 51 $\times$ 51 pixels. The two stationnary sources radiate at 1500 Hz and a random uniformely distributed noise of (SNR=20 dB) is added to the signal measured by each microphone. In the following, three algorithms are compared for the identification of the velocity field, namely: Beamforming (BF) as presented in Eqn. 10, Pseudo-Inverse using the truncated SVD of $[\mathbf{G}]$ according to Eqn. 5 (PI_{SVD}) and the iterative Phase Coherence Algorithm (iPCA).

$$v_s^{\text{BF}} = \frac{2\pi}{A_e j\omega\rho_0 M} \sum_{m=1}^{M} \frac{p_m G_{ms}^*}{|G_{ms}|^2} \tag{10}$$

As shown on the left part of Figure 6, at the first iteration (first use of the phase coherence thresholding), the iPCA rejects approximately half the pixels of the imaging domain (white pixels). This means that the resolution using the regularized pseudo-inverse of $[\mathbf{G}]$ on this new imaging domain is already faster when compared with the standard PI_{SVD}. After only a few iterations the imaging domain converges toward the extent of the two pistons, resulting in approximately a domain of one tenth the size of the original domain containing only active elements. The right part of Figure 6 shows the normal velocity evaluation of the whole imaging domain given the domain obtained at the last iteration.

From Figure 6, the velocity field evaluated using the iterative algorithm corresponds to the instantaneous velocity of a snapshot at time $t = 0$ of both pistons ($0.01e^{j\pi/3} = 0.05$ m and $0.01e^{j2\pi/3} = -0.05$ m) . Moreover, it is clear that the boundaries of the two pistons are well identified. To help visualizing the advantage of the iterative PC algorithm, the amplitude of the velocity field (in dB) and the instantaneous phase maps are presented in Figure 7 for the BF, the PI_{SVD} and the iPCA algorithms respectively.

It is clear from Figure 7 that the three presented algorithms localize the two pistons (and their absolute phases) with good precision. However, the magnitude maps provided by the BF and

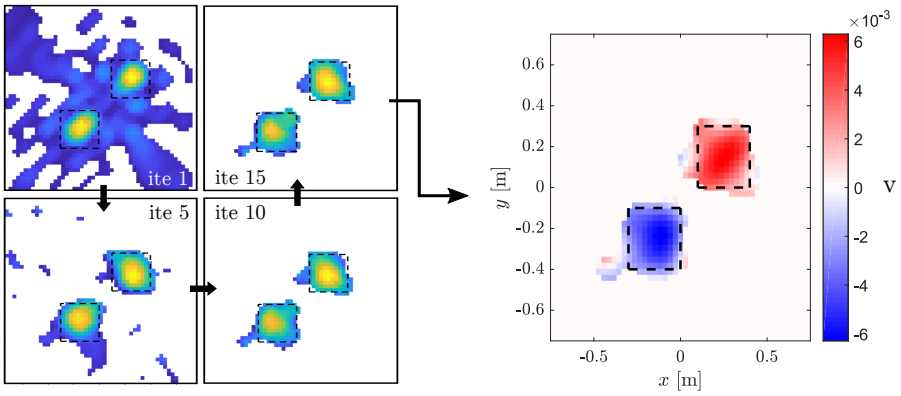

Figure 6: (left) Pixel rejection process and identification of the boundaries of the pistons using the iPCA algorithm and (right) resulting velocity map obtained after 15 iterations

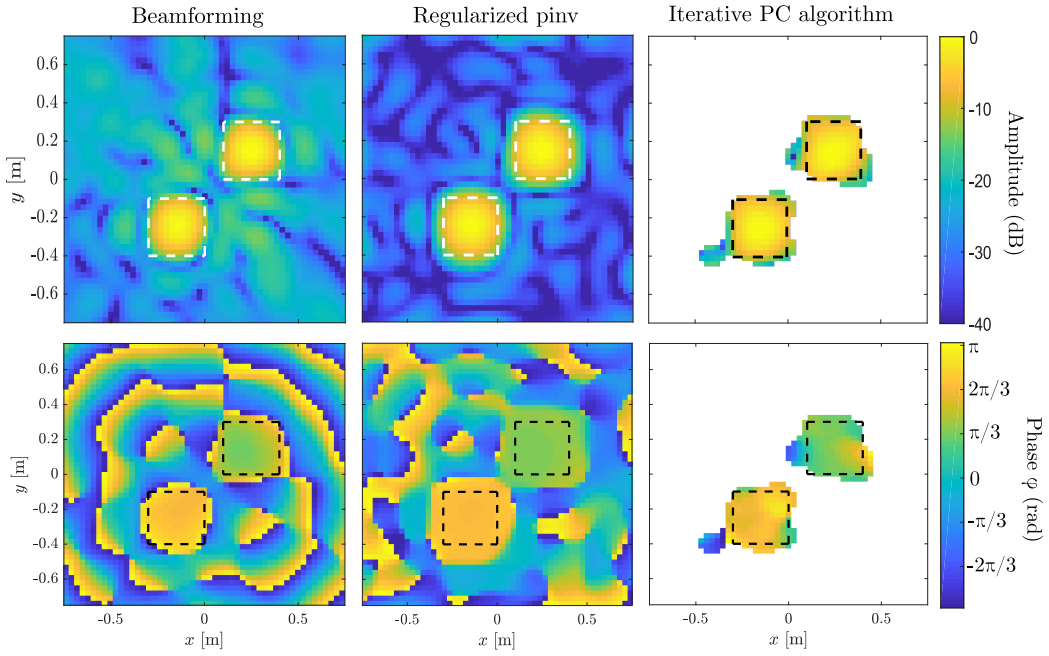

Figure 7: Velocity magnitude in dB (top row) and instanteneous phase map (bottom row) obtained with the BF, PI_{SVD} and iPCA respectively.

PI_{SVD} algorithms show important artefacts (sidelobes). The dynamic range of the magnitude map obtained with the PI_{SVD} is larger than the one from the BF. Such artefacts are not present on the magnitude map obtained using the iPCA since the thresholding on the phase coherence rejected these pixels in the iterative process. Moreover, this pixel rejection process considerably improves the localization of the boundaries of the radiating elements. In order to show the potential of evaluating the acoustic radiated power using the iPCA, the presented tools are applied to the case of a simply-supported vibrating plate in the next section.

3.2 Simply-supported plate

For the following, a simply-supported baffled plate excited using a point force is considered. The velocity of the structure is obtained using the modal summation method:

$$v(x,y) = \sum_{m=1}^{\infty} \sum_{n=1}^{\infty} u_{mn} \phi_{mn}(x,y) \tag{11}$$

where u_{mn} is the velocity amplitude of mode (m,n) and ϕ_{mn} is the shape of mode (m,n) as defined in [11]. Let's consider an aluminium plate with a thickness of 2 cm, width (x axis) of 48 cm and length (y axis) of 42 cm, centered on the imaging domain and excited at the natural frequency of its (2,2) mode. The amplitude (in dB) and phase of the velocity field reconstructed from th BF, PI_{SVD} and iPCA are presented in Figure 8 for a regular array (11×11 microphones) positionned at $z_m = 1.5$ m above the structure and for a SNR of 14 dB.

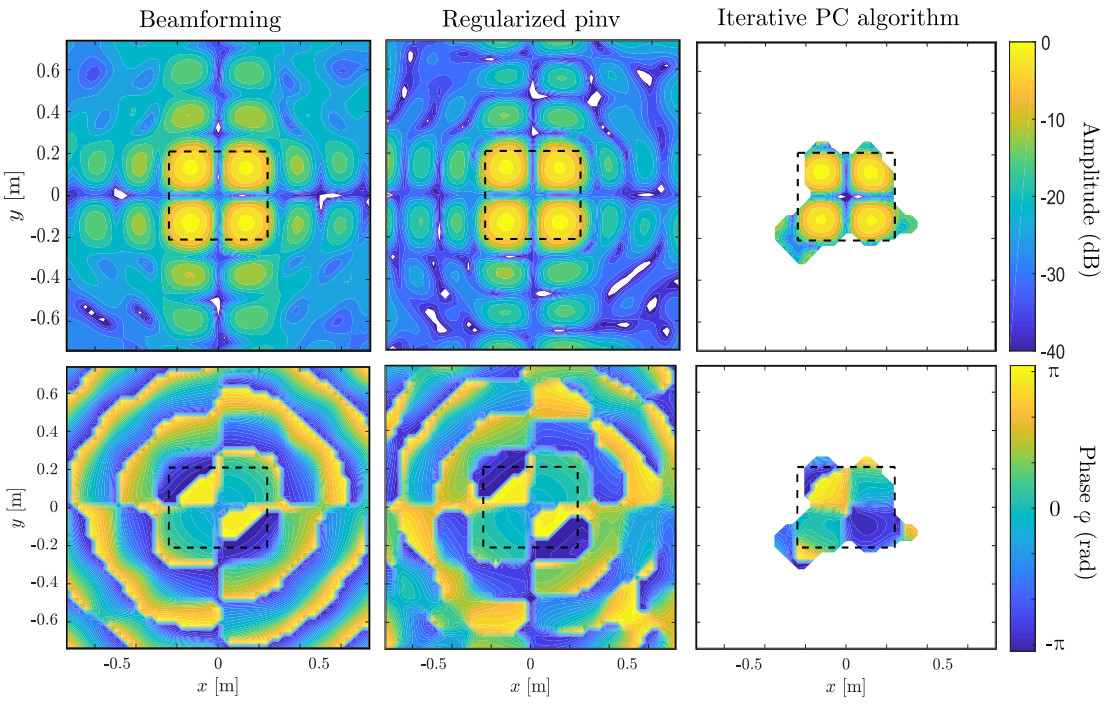

Figure 8: Velocity magnitude in dB (top row) and instanteneous phase map (bottom row) obtained with the BF, PI_{SVD} and iPCA respectiveley for the simply-supported plate

Like in case of the stationnary pistons, it is possible to observe from Figure 8 that the iPCA correctly identifies the boundaries of the structure (represented by the dashed line). Indeed, the points with low phase coherence (where no active source is present) are neglected in the resolution of Eqn. 5. Consequently, a large dynamic range is obtained for the velocity magnitude map and no sidelobes are observed. Moreover, the spatial resolution obtained using the iPCA is better than for the two other algorithms. Indeed, the main lobes provided by the iPCA coincide with the 4 antinodes of the stationnary source and do not extend over the boundaries of the plate. This better identification of the velocity field helps evaluating the total radiated acoustic power.

Indeed, as presented in Figure 9(c), the algorithm converges toward a closer value to the exact radiated acoustic power (for this given configuration) than the regularized method. Acoustic power estimations for configurations associated to different conditionning of $[\mathbf{G}]$ are presented in Figure 9.

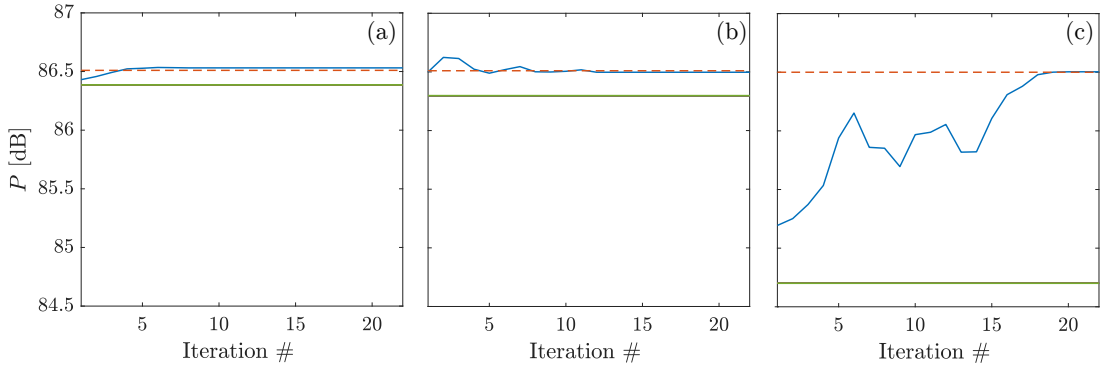

Figure 9: Radiated power estimation by the PI_{SVD} (green line), the iPCA (blue line) and exact value (dashed line) for three different configurations: (a) SNR=20 dB and $z_m = 0.8$ m, (b) SNR=14 dB and $z_m = 0.8$ m and (c) SNR=14 dB and $z_m = 1.5$ m

As presented in Figure 9(a), the PI_{SVD} and iPCA give correct estimations of the total radiated power when the vibrating structure is a few wavelengths away from the array ($0.8\ m\ \approx 4\lambda$) and for a random (uniformely distributed) added noise resulting in a SNR of 20 dB. Figure 9(b) shows that when measurement noise increases, the PI_{SVD} estimation of the total radiated power becomes slidghtly less precise. Moreover, the iPCA converges slightly more slowly toward the exact value. Finaly, Figure 9(c) shows that when the array is moved away from the vibrating structure, the same observations as for Figure 9(b) occur. Indeed, an increase in z_m results in an increase of the conditioning number of $[\mathbf{G}]$. This bad conditionning results in stronger sensitivity to noise and in a power estimation error of about 2 dB for the PI_{SVD} algorithm. However, using the iterative algorithm, the reduced imaging domain regularizes the inversion and results in a correct evaluation of the acoustic radiated power. The number of required iterations is however increased to 18 iterations before convergence. Although, moving the array further away from the source ($z_m > 1.5$ m) results in a wrong evaluation of the acoustic radiated power from both methods since part of the radiated energy is directed away from the extent of the antenna.

4 Conclusion

A new algorithm for vibroacoustic imaging and acoustic power estimation is herein presented. The algorithm iteratively rejects points of the imaging domain for which the phase coherence between the microphones is low. This results in a smaller linear system to solve and a better estimation of the velocity field when compared to the resolution using the regularized pseudo-inverse. It was shown that as the conditionning of $[\mathbf{G}]$ gets worst, the gain of using the phase coherence algorithm before the regularized pseudo-inverse increases. Future work will be oriented toward a time domain formulation in order to adapt the algorithm to non stationnary vi-

broacoustic sources. The use of spatial coherence, phase coherence and time averaging should lead to betteridentification of the boundaries od extended sources.

References

[1] D. Blacodon and G. Elias. Level Estimation of Extended Acoustic Sources Using a Parametric Method. *Journal of Aircraft*, 41(6), 2004.

[2] S. Marburg. Surface contributions to radiated sound power. *The Journal of the Acoustical Society of America*, 133(6), 2013.

[3] G. Chardon, L. Daudet, A. Peillot, F. Ollivier, N. Bertin, and R. Gribonval. Near-field acoustic holography using sparse regularization and compressive sampling principles. *The Journal of the Acoustical Society of America*, 132(3):1521–1534, 2012.

[4] W. Xiong. *Localisation de sources dispersées : Performances de MUSIC en présence d'erreurs de modèle et estimation à rang faible* . PhD thesis, 2016.

[5] J. Abou, J. Picheral, and S. Marcos. Localization of spatially distributed near-field sources with unknown angular spread shape. *Signal Processing*, 106:259–265, 2015.

[6] J F Cruza, J Camacho, and C Fritsch. Plane-wave phase-coherence imaging for NDE. *NDT and E International*, 87(December 2016):31–37, 2017.

[7] Peter Kovesi. Phase congruency: A low-level image invariant. *Psychological Research-Psychologische Forschung*, 64(2):136–148, 2000.

[8] Y. Shechtman, Y C. Eldar, O. Cohen, H N. Chapman, J. Miao, and M. Segev. Phase Retrieval with Application to Optical Imaging: A contemporary overview. *IEEE Signal Processing Magazine*, 32(3):87–109, 2015.

[9] A. V. Oppenheim and J. S. Lim. Importance of Phase in Signals. *Proceedings of the IEEE*, 69(5):pp. 529–541, 1980.

[10] J. Camacho and C. Fritsch. Phase Coherence Imaging. *IEEE Transactions on Ultrasonics, Ferroelectrics and Frequency Control*, 56(5):958–974, 2009.

[11] A. Putra and D. J. Thompson. Sound radiation from rectangular baffled and unbaffled plates. *Applied Acoustics*, 71(12):1113–1125, 2010.

[12] A. Pereira. *Acoustic imaging in enclosed spaces*. PhD thesis, 2013.

[13] S.H. Yoon and P.A. Nelson. Estimation of Acoustic Source Strength By Inverse Methods: Part II, Experimental Investigation of Methods for Choosing Regularization Parameters. *Journal of Sound and Vibration*, 233(4):665–701, 2000.

[14] F. Fahy and P. Gardonio. *Sound and structural vibration - Radiation, Transmission and Response*. Second edition, 2007.